Calculation of Rigid-Body Conformational Changes Using Restraint-Driven Cartesian Transformations

Pornthep Sompornpisut, Yi-Shiuan Liu, and Eduardo Perozo
Department of Molecular Physiology and Biological Physics, University of Virginia Health Sciences Center, Charlottesville, Virginia 22906-0011 USA

ABSTRACT We present an approach for calculating conformational changes in membrane proteins using limited distance information. The method, named restraint-driven Cartesian transformations, involves 1) the use of relative distance changes; 2) the systematic sampling of rigid body movements in Cartesian space; 3) a penalty evaluation; and 4) model refinement using energy minimization. As a test case, we have analyzed the structural basis of activation gating in the *Streptomyces lividans* potassium channel (*KcsA*). A total of 10 pairs of distance restraints derived from site-directed spin labeling and electron paramagnetic resonance (SDSL-EPR) spectra were used to calculate the open conformation of the second transmembrane domains of *KcsA* (TM2). The SDSL-EPR based structure reveals a gating mechanism consistent with a scissoring-type motion of the TM2 segments that includes a pivot point near middle of the helix. The present approach considerably reduces the amount of time and effort required to establish the overall nature of conformational changes in membrane proteins. It is expected that this approach can be implemented into restrained molecular dynamics protocol to calculate the structure and conformational changes in a variety of membrane protein systems.

INTRODUCTION

Site-directed spin labeling, in combination with electron paramagnetic resonance spectroscopy (SDSL-EPR) has become a powerful tool in obtaining structural and dynamical information of both soluble and membrane proteins of arbitrary size (Hubbell and Altenbach, 1994; Hubbell et al., 1998, 2000). In particular, SDSL-EPR has been quite successful in identifying secondary structure elements and tertiary folds in membrane protein systems (Perozo et al., 1998; Poirier et al., 1998; Koteiche and McHaourab, 1999; Cortes et al., 2001).

In SDSL, a nitroxide spin probe is covalently attached into a given site in a protein by changing that particular residue to cysteine via standard mutagenesis methods, followed by covalent attachment of a nitroxide moiety using sulfhydryl chemistry. Typically, a methanethiosulfonate-based spin label (MTSSL) is used due to its high reactivity and specificity toward free sulfhydryl groups (Fig. 1 *A*). Once the spin label is incorporated into the target cysteine, detection of the local EPR signal allows for a detailed structural characterization of the environment surrounding a particular position.

Using SDSL-EPR, the dynamics and structural information of a protein can be obtained through the analysis of three different experimental parameters: probe mobility, solvent accessibility, and inter-spin distances (Hubbell et al., 1998). The first two parameters are sequence dependent and can be used to draw local secondary structure and help infer tertiary or quaternary contact points in proteins. Distance information can be extracted from the extent of spectral broadening due to through-space electron-electron dipolar interactions (Likhtenshtein, 1976; Eaton and Eaton, 1989; Rabenstein and Shin, 1995; Hustedt et al., 1997; Steinhoff et al., 1997). Inter-spin distances can be estimated in the range of 8 to 25 Å using a number of approaches, including Fourier deconvolution methods (Rabenstein and Shin, 1995; Steinhoff and Hubbell, 1996) and the global analysis of mutifrequency spectra (Hustedt et al., 1997).

By combining multiple SDSL-EPR data, it is possible to develop a strategy to determine protein folds at the backbone level (Mchaourab and Perozo, 2000). However, given the significant investment in labor and costs necessary to engineer the large numbers of labeling sites required to fully explore the conformational space of a protein of unknown structure, traditional approaches used to compute solution structures are not compatible with the limited number of SDSL-EPR data. Therefore, an alternative approach needs to be developed to efficiently use EPR data in the determination of protein folds and conformational rearrangements in proteins.

Molecular modeling of integral membrane proteins is regarded as considerably less challenging than that of soluble proteins due to the large energetic restrictions imposed by the lipid bilayer (Bowie, 1997a,b; Booth and Curran, 1999; Pappu et al., 1999; White and Wimley, 1999; Capener et al., 2000). Membrane proteins reach the proper molecular conformations with limited folding solutions. Because of the influence of hydrophobic protein-lipid interactions, the specific requirements of transmembrane helix packing are typically used, providing powerful constraints in structure prediction of membrane proteins (Donnelly et al., 1993; Son

Received for publication 27 April 2001 and in final form 25 July 2001.

Address reprint requests to Dr. Eduardo Perozo, University of Virginia, Department of Molecular Physiology and Biological Physics, Box 449, Jordan Hall, Charlottesville, VA 22906-0011. Tel.: 804-243-6580; Fax: 804-982-1616; E-mail: eperozo@virginia.edu.

Pornthep Sompornpisut is on leave from Department of Chemistry, Faculty of Science, Chulalongkorn University, Bangkok, Thailand.

0006-3495/01/11/2530/17 $2.00

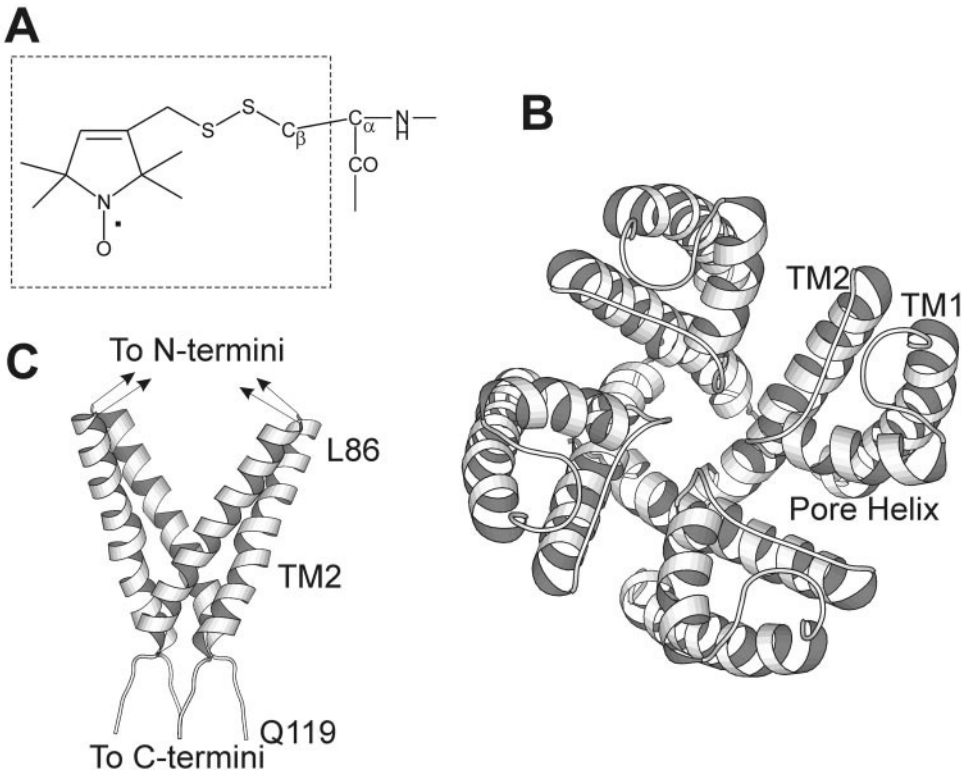

FIGURE 1 (*A*) Methanethiosulfonate spin label sidechain; (*B*) *KcsA* x-ray structure; (*C*) *KcsA* TM2 segments. *B* and *C* were generated using the program Molscript (Kraulis, 1991).

and Sansom, 1999). By combining this knowledge basis with structural data from experimental techniques, the generation of membrane protein folds can be significantly simplified, a fact that must be taken into consideration for the analysis of the vast amounts of genomic data coming from massive sequencing projects.

There are a number of examples in which membrane protein modeling has been pursued using a limited number of experimental structural restraints. This includes various conformational search algorithms such as simulated annealing with Monte Carlo, with molecular dynamics (SA/MD), or with distance geometry protocols (Herzyk and Hubbard, 1995; Sansom et al., 1995; Pogozheva et al., 1997; Sansom, 1998). In these approaches, the α-helix serves as a template transmembrane conformation for each system.

The evaluation of transmembrane helix packing solutions is mostly based on penalty calculations or potential energy functions. For instance, an SA/MD technique incorporating distance restraints derived from mutagenesis data was used to model the closed conformation of the pore domain of the nicotinic acetylcholine receptor (Sansom et al., 1995). The structure of a tetrameric transmembrane H^+ channel from the influenza A virus was modeled by adding the potential term for the helical orientation derived from site-directed infrared dichroism data into the MD calculations (Kukol et al., 1999). Simulated annealing with Monte Carlo was used to model the arrangement of the seven transmembrane helices of bacteriorhodopsin on the basis of potential calculations (Son and Sansom, 1999). By considering theoretical and experimental data within a rigid body assembly, a number of membrane proteins have been modeled (Herzyk and Hubbard, 1995, 1998). It should be noted that the latter technique made use of restraints based on SDSL-EPR accessibility data. Recently, spin probe mobility, accessibility parameters, and interspin interaction parameters of the N- and C-termini of the K^+ *KcsA* channel were incorporated as structural restraints in SA/MD calculations, resulting in a three-dimensional folding model of the full-length potassium channel (Cortes et al., 2001).

The bacterial K^+ channel from *Streptomyces lividans KcsA* is a homo-tetrameric integral membrane protein in which each subunit contains two transmembrane (TM) domains cradling a pore region that includes the signature sequence (GYGD) critical for ion permeation and selectivity (Doyle et al., 1998). Because of the functional importance of potassium channels, the availability of the *KcsA* crystal structure (Fig. 1 *B*) has prompted a number of theoretical studies, trying to extend the structural description of the ion permeation and selectivity mechanisms (Roux and MacKinnon, 1999; Allen et al., 2000; Aqvist and Luzhkov, 2000; Berneche and Roux, 2000; Guidoni et al., 2000; Shrivastava and Sansom, 2000). Evidence from ion flux experiments and electrophysiological and EPR

TABLE 1 Experimental interspin distance dataset (r_{open} and r_{closed}) and the distance changes of two diagonal subunits of (Δr_{epr})

	I100C	F103C	T107C	A108C	A109C	T112C	V115C	G116C	R117C	Q119C
r_{closed} (Å)	14.9	19.5	11.4	9.7	>25*	8.5	10.3	9.4	16.8	11.4
r_{open} (Å)	12.2	23.9	11.3	10.5	15.6	11.4	15.9	15.7	24.8	15.5
Δr_{epr} (Å)	−2.7	4.4	−0.1	0.8	<−9.4	2.9	5.6	6.3	8.0	4.1

*There is no measurable dipolar broadening in the closed state, and the lower distance bound was not used.

studies suggested that the conformation of the crystal structure corresponds to a closed state, that the open state can be stabilized at low pH, and that the activation gating is associated with a significant structural rearrangement of the two transmembrane domains (Cuello et al., 1998; Perozo et al., 1998, 1999). However, the structural details of the open channel conformation are yet to be described, owing to the current lack of high-quality crystals of *KcsA* in acidic pH and to the fact that the size of *KcsA* makes it too large to be analyzed by solution nuclear magnetic resonance (NMR) methods.

This report presents an approach we call restraint-driven cartesian transformations (ReDCaT) in which a limited number of distance restraints have been used to determine conformational changes in membrane protein systems. As a test case, we have analyzed the structural basis of activation gating in the potassium channel *KcsA*. We have focused our analysis on the structural rearrangement of the second transmembrane segments (TM2, Fig. 1 *C*) because of its functional significance and its strategic location near the predicted fourfold axis of symmetry. We show that the ReDCaT approach is a useful alternative in the determination of conformational changes in membrane proteins. The relativity simplicity of its implementation, its low computational cost, and the overall robustness of the method (derived from an analysis of the sensitivity to the number and location of the restrains) makes ReDCaT an ideal choice in combination with reporter-group-based structural constraints.

MATERIALS AND METHODS

Experimental methods

Sample preparation

Design, expression, and characterization of *KcsA* tandem dimer mutants have been described in detail by Liu et al. (2001). Briefly, tandem dimers were constructed with different oligopeptide linkers, having rTEV protease recognition site in a pQE-32-based *KcsA* vector (Cortes and Perozo, 1997). This resulted in pseudo-tetrameric cysteine mutants of *KcsA*. Expression of *KcsA* and tandem dimers was followed using the protocol described by Cortes et al. (1997). A cobalt-based metal chelate chromatography was used to purify the protein sample.

EPR spectroscopy and distance determination

Reconstituted samples were spin labeled with MTSSL as described in Liu et al. (2001). The spectra were obtained from an EMX X-band EPR spectrometer (Bruker Instruments, Billerica, MA) with loop-gap resonator at 50 μW of microwave power and 1-G field modulation (100 kHz) at 150 K. From the relation of the average magnetic field splitting, the distance measurement can be estimated through the dipolar broadening function (B) using Fourier deconvolution method (Rabenstein and Shin, 1995).

$$B = F^{-1}\{F(D)/F(S)\} \tag{1}$$

In practice, B is obtained from the inverse Fourier transform (denoted by F^{-1}) of the division of the Fourier transform of the fully (double)-labeled spectra ($F(D)$) by that of the under (single)-labeled spectra ($F(S)$). The EPR spectra of the fully- and under-labeling mutants recorded at two different pH conditions were analyzed to obtain interspin distances between diagonal TM2 subunits.

Computational details

The method can be divided into three main steps: 1) defining distance restraints; 2) performing ReDCaT; and 3) refinement of the calculated ReDCaT conformers. Details of these steps are described below.

Restraints

For a residue i^{th}, the upper ($\Delta r_{upl}(i)$) and lower ($\Delta r_{lol}(i)$) bounds for the experimental distance changes between diagonal subunits are defined by

$$\Delta r_{lol}(i) = \Delta r_{epr}(i) - 2\delta$$

$$\Delta r_{upl}(i) = \Delta r_{epr}(i) + 2\delta \tag{2}$$

$$\Delta r_{epr}(i) = r_{open}(i) - r_{closed}(i) \tag{3}$$

in which $\Delta r_{epr}(i)$ is the distance change of the residue i^{th} calculated by the subtraction of the EPR interspin distance in the open state from that of the closed state. The distance deviation factor, δ, was introduced to define a range between the upper and lower limits of the restraints. δ was parameterized on the basis of the estimated experimental deviation for the interspin determination from EPR spectra and was varied to estimate its optimal value. Eqs. 2 and 3 were applied on all 10 distance datasets (Table 1), giving rise to the SDSL-EPR restraints.

ReDCaT protocol

The flowchart of the ReDCaT method is shown in Fig. 2. The x-ray coordinates of the bacterial potassium channel at the atomic resolution of 3.2 Å was obtained from the Research Collaboratory for Structural Bioinformatics (www.rcsb.org) with the PDB code 1bl8 (Fig. 1 *B*) (Doyle et al., 1998). Each TM2 segment contains 34 amino acids, where L86 and Q119 cap the N and C termini, respectively (Fig. 1 *C*). The known three-dimensional structure was used both as a structural template and as the reference Cα-Cα distances in the closed state. Fig. 3 illustrates how the structural coordinates were transformed before implementation into in ReDCaT. The result from the subtraction of the distances between the reference and the generated configuration was used to calculate the penalty parameter. Description of the two main routines, configuration generation and penalty calculation, follows.

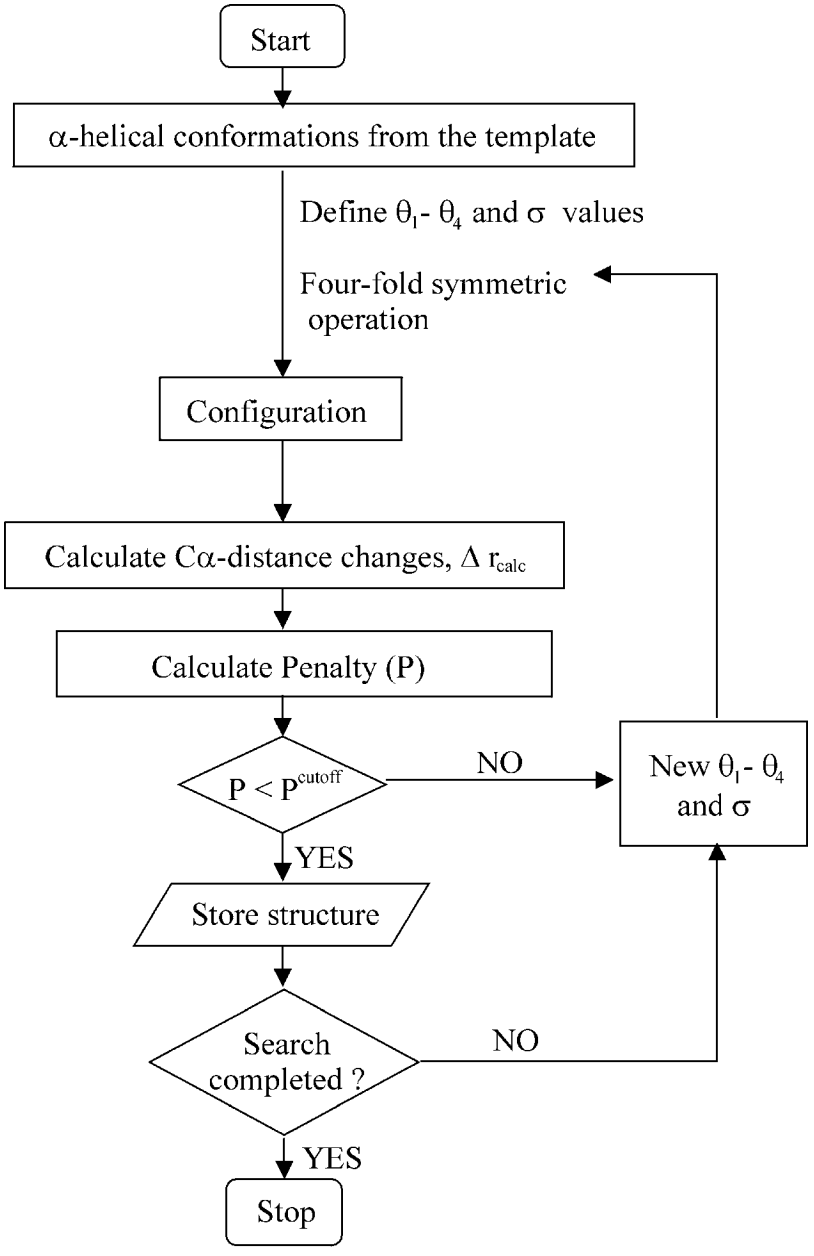

FIGURE 2 Flowchart of the ReDCaT protocol.

Configuration generation

The procedure used to generate the configuration of the tetrameric system follows assumptions of rigid body rearrangements and symmetric relationships. All x-ray atomic coordinates belonging to the TM2 segment of the subunits A, B, C, and D of the reference structure were transformed into a new Cartesian coordinate frame. The transformed coordinates in the new frame were generated in such a way that the virtual fourfold axis of symmetry is aligned to the z axis, whereas the $\pm x$ and $\pm y$-axes pass through the defined rotating center of the individual subunit (Fig. 3 *A*). Here, the vector of the core axis is essentially normal to the membrane bilayer, and each segment has its own vector as the TM2 α-helix representation. The position of each TM element is defined by the transformation of the local x, y, and z, where the origin of the local axes was placed at the center of the rotation (Fig. 3 *B*). This allows for an easy way to manipulate configurations of the system and helps further structural analysis. There are two pieces of evidence supporting the view that conformational changes in *KcsA* involve rigid body rearrangements of the TM segments. On one hand, the circular dichroism and Fourier transform infrared studies suggest that the closing and opening of the channel is not accompanied by substantial changes in the secondary structure content of the channel (Tatulian et al., 1998, Perozo et al. 1999). Additionally, Fourier analysis of EPR data periodicities showed that angular frequencies derived from sequential mobility and spin coupling measurements along TM2 do not change significantly upon channel opening (Perozo et al. 1999). In view of this evidence, the dihedral angles of each subunit were kept fix during sampling configurations.

Multiple configurations of this system can be generated by varying a total of five degrees of freedom that include four rotations (θ_1–θ_4) and one

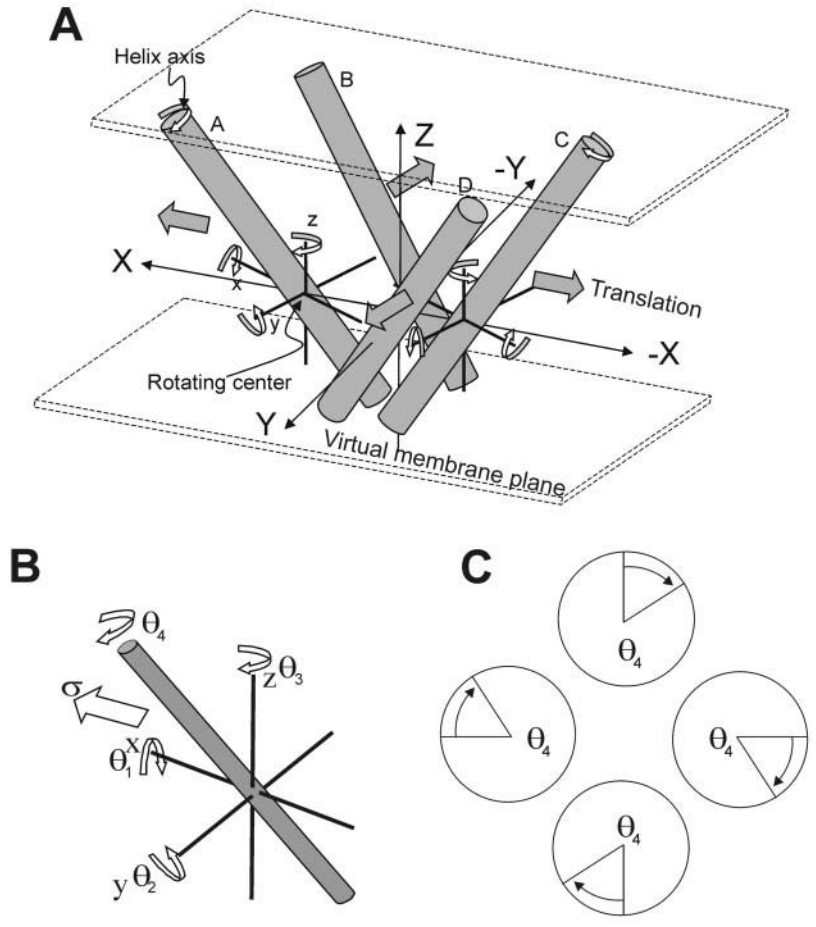

FIGURE 3 Graphical representation of rigid body TM2 bundles and definition of degrees of freedom: (*A*) the rotation and the translation applied to the four segments symmetrically (the *z* axis is also the axis of molecular symmetry); (*B*) rotational ($\theta_1-\theta_4$) and translational (σ) parameters for each individual segment in the local axis; (*C*) a rotation (θ_4) on the segment itself (projection on the main helical axis).

translation (σ). Each rigid body element was subjected to rotation with angles θ_1, θ_2, and θ_3 along the local *x*-, *y*-, *z*-axes, respectively (Fig. 3 *B*), whereas the θ_4 was applied to rotate TM2 segments about its helical vector (Fig. 3 *C*). Combined with a lateral of the translation parallel to the plane of the bilayer, adequate sampling of the different configurations can be achieved. Equivalent changes of these five parameters were applied to each subunit to maintain the channel symmetry.

Next, the range and the step size of these parameters is defined. The range for θ_1 and θ_2 rotations was limited to within 0 and π, whereas θ_3 and θ_4 were allowed to vary between 0 and 2π. For σ, a range of 0 to 40 Å is defined. The step size was 10° for all rotations/tilts and 0.4 Å for the lateral translation. These increments were tested and found to provide efficient conformational search within a reasonable three-dimensional boundary and prevent the generation of mirror-image structures. Under these conditions, a single run generates a total of approximately forty million configurations, a number that can be easily handled by a Pentium III personal computer.

Penalty function

The penalty function, *P*, is defined by a sum of the distance violations of the restrained residues. The penalty function is given by:

$$P = \sum k \cdot viol^2 \tag{4}$$

viol

$$= \begin{Bmatrix} \Delta r_{\text{calc}}(i) - \Delta r_{\text{upl}}(i); & \Delta r_{\text{calc}}(i) > \Delta r_{\text{upl}}(i) \\ \Delta r_{\text{lol}}(i) - \Delta r_{\text{calc}}(i); & \Delta r_{\text{calc}}(i) < \Delta r_{\text{lol}}(i) \\ 0; & \Delta r_{\text{lol}}(i) \le \Delta r_{\text{calc}}(i) \le \Delta r_{\text{upl}}(i) \end{Bmatrix} \tag{5}$$

in which *viol* and *k* are the violation and the constant of the restrained residue i^{th}, respectively. The parameter *k* is an arbitrary value and is used as a weighting factor. Distance changes calculated from the configuration and the reference x-ray structure, Δr_{calc}, are in a form of:

$$\Delta r_{\text{calc}}(i) = \bar{r}_{\text{calc}}(i) - \bar{r}_{\text{ref}}(i) \tag{6}$$

in which $\bar{r}_{\text{ref}}$ and $\bar{r}_{\text{calc}}$ are, respectively, the average Cα-Cα distance of the reference and the generated configuration from both pairs of diagonal subunits (A-C and B-D) in the system. Δr_{upl} and Δr_{lol} were taken from Eq. 2 described in the previous section.

Refinement

Because the lowest penalty ReDCaT structures are not calculated taken into account their conformational energy, it is essential to subsequently

TABLE 2 Penalty ratio and RMSD of the 25 ReDCaT structures of R1 to R6

	R1	R2	R3	R4	R5	R6
δ (Å)	1	1	0.5	1.5	2	2.5
Penalty ratio*	1	0.77	1.74	0.24	0.04	1.70E-04
RMSD (Å)	1.27 ± 0.8	0.91 ± 0.4	0.94 ± 0.5	0.96 ± 0.5	1.51 ± 1.0	2.42 ± 1.6

*For calculating the penalty ratio, the absolute penalty from the R# is divided by the absolute penalty obtained from the R1.

refine a given ensemble to prevent steric clashes that will lead to energetically unfavorable conformations. In the refinement stage, full atomic models were used by this purpose. Fifty ReDCaT structures generated from the two best runs R2 and R4 (see Results for definitions) were subjected to energy minimization. Sidechain conformations were assigned according to the x-ray internal coordinates. The missing sidechain of R117 was built based on the Amber amino acid library. Hydrogen atoms were added taking into account charged residues, which presumably hold a positive charge for R89 and R117 and a negative charge for E118. All energy calculations were performed using the program Amber 6 (Case et al., 1999) with the Cornell force field for proteins (Cornell et al., 1995).

The 50 structures were subjected to energy minimization with a total of 5000 steps of steepest descent and then conjugate gradient methods. The cutoff distance for nonbonded interactions was 12 Å, and a distance-dependence dielectric was used throughout the refinement. After that, an average structure was computed from the family and then energetically minimized once again. The final refined structure was obtained after this step. Protein structures were displayed and analyzed using the program Procheck-NMR (Laskowski et al., 1996), Rasmol (Sayle, 1994), Molmol (Koradi et al., 1996), and Weblab Viewer (Accelrys Inc., San Diego, CA).

RESULTS

EPR and distance measurements

Being a homotetramer, wild-type *KcsA* cannot be used in the determination of intersubunit distances because the combination of spin-spin dipolar interactions from next neighboring and diagonally related subunits results in nonreliable distance data. This interference can be eliminated using a tandem dimer constructs so that only two identical residues located in diagonal subunits are available for spin labeling. This allows the measurement of interspin distances from dipolar couplings from two unpaired electrons instead of four (Liu et al., 2001). Absorption EPR spectra were obtained, and the diagonal inter-subunit distances between two spin-labeled residues were calculated (Table 1) under conditions that stabilize the closed (pH 7.0) and the open state (pH 4.0). Experimental details and interpretation of these data have been described elsewhere (Liu et al., 2001).

Tests of the methodology

We tested the approach by running a ReDCaT series with the following objectives: 1) seeking an appropriate distance range between the upper and the lower bounds; 2) examining the reliability of the method; and 3) testing the sensitivity of the restraints. To accomplish these goals, a number of independent runs include: 1) varying the distance deviation parameter δ; 2) determining the closed bundle structure by reversing the value of the constraints and comparing the result of the calculation with the reference x-ray structure; 3) changing the helix center of rotation; and 4) assessing the relative importance of individual SDSL-EPR restraints. For simplicity, each run is denoted as R# (see context for details). Twenty-five structures having the lowest penalty values were selected in each of the runs. For structural comparison, the global root-mean-square deviation (RMSD) from an ensemble of 25 structures, and the pairwise RMSD (between the two average structures of different ensembles) for the backbone atoms were used unless stated otherwise. The symbol ⟨R#⟩ denotes the average structure from the ensemble.

Starting a reference run

A total of 10 SDSL-EPR restraints (Table 1) were incorporated in the R1 run. Based on the reported distance deviations determined from continuous wave-EPR spectra (Rabenstein and Shin, 1995), the δ value was initially set to 1 Å, giving rise to a 4-Å spread in the distance range of SDSL-EPR restraints (Eq. 2 in Materials and Methods). The force constant, k (Eq. 4), was set to 50 $Å^{-2}$. As shown in Table 2 and Fig. 4 *A*, the RMSD of the ensemble of the resulting 25 ReDCaT structures from this run was 1.27 ± 0.8 Å. Thus, using a small number of restraints the ReDCaT strategy was able to generate structures with a low RMSD. It should be noted that for this initial run (R1) the deviation in the global RMSD values (±0.8 Å) stems from the conformational differences between two apparent clusters (with ~0.3 and 0.7 probability, respectively) within the ensemble (Fig. 4 *A*). The RMSD between the clusters is approximately over 2 Å. The structures of the two clusters are well defined around the cytoplasmic end of TM2 domains (residue 104–119), whereas the structural convergence of its N-terminal half (residue 86–103) is relatively poor. Clearly, this stems from the fact that most of the restrained residues are located near the cytoplasmic half of TM2.

Reducing the restraining constant of residues 117 and 119

As described in the Materials and Methods section, all reference distances were obtained from the *KcsA* x-ray structure. This structure was obtained after chymotrypsin

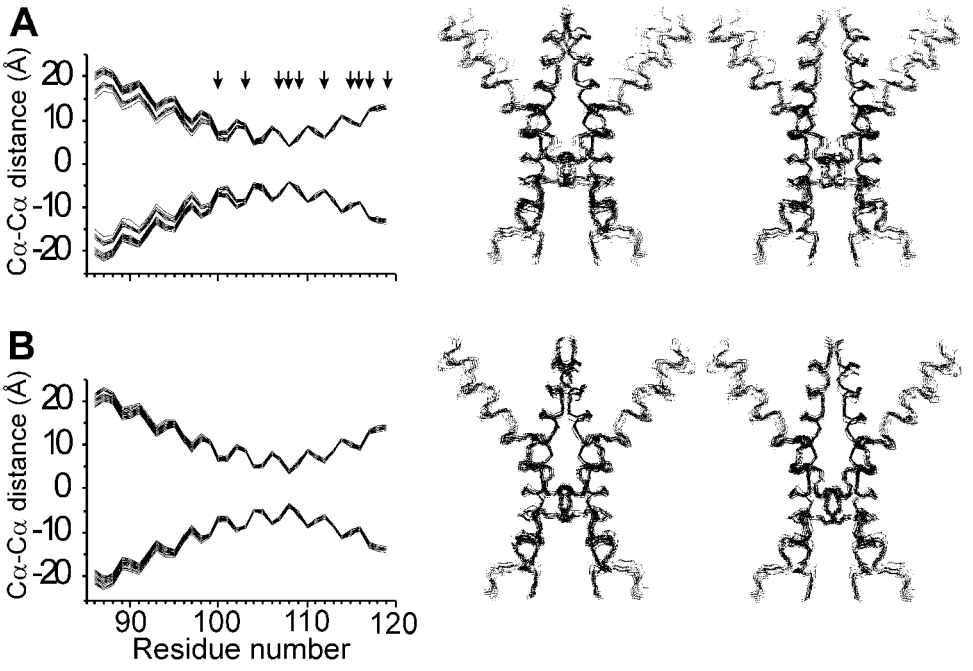

FIGURE 4 Two-dimensional projection of the per-residue α-carbon diagonal subunit distance (*left*) and a backbone stereo view of the corresponding 25 ReDCaT conformers generated using the program MolMol (Koradi et al., 1996) (*right*): R1 (*A*) and R2 (*B*). The arrows indicate residues from which experimental EPR data were used as ReDCaT restraints.

treatment of full-length channel, which renders a channel with its C-terminus truncated near residue 125 (Doyle et al., 1998). Experimental evidence on the functional consequences of the chymotrypsin cut in *KcsA* indicates that the C-terminus can influence pH dependence of activation gating and can affect the dynamics of the cytoplasmic end of TM2 (Cortes et al., 2001). Given that all the EPR-based distance information used as constraints in ReDCaT was obtained from full-length channels, we have taken into consideration possible edge effects in the x-ray coordinates due to the chymotrypsin cut by allowing some additional softness in the restraints around this region. This was done in the second run R2 by decreasing the weighting restraining constant k for the last two distance restraints at positions 117 and 119 (the k value was decreased $\sim$5 times as compared with the R1 run).

The global RMSD was 0.91 $\pm$ 0.4 Å, a considerable improvement in terms of the precision of the ensemble of the structures in relation to R1 (Table 2). In this case all 25 ReDCaT conformers were well defined and fall into single cluster (Fig. 4 *B*). This ensemble is similar to the more populated cluster obtained from R1 as judged by the 0.83-Å pairwise RMSD between the average structures of the two families (R2 and R1). Here we used the dataset and the resulting structures of R2 to serve as internal control for further tests.

Parameterization of δ

The δ parameter defines the allowed range in the upper and the lower limits of the distance constraints. In an attempt to determine the sensitivity of the ReDCaT approach to the uncertainty in the EPR-derived distances, we have systematically varied δ to determine its effect on the structure convergence.

Search conditions used in R3 to R6 were the same as those of R2, except for the SDSL-EPR restraints. The distance range of the restraints was varied within 2, 6, 8, and 10 Å corresponding to δ of 0.5, 1.5, 2.0, and 2.5, respectively. The results of this test are presented in Fig. 5 *A* and Table 2. The global RMSD of these runs increase from 0.94 to 2.42 Å. The ensembles of R2, R3, and R4 are quite similar to each other, whereas R5 and R6 failed to converge as a consequence of the wider restraints. The Cα profiles of R3 and R4 with respect to that of R2 were very similar with a range of 0.12 to 0.27 Å for the pairwise RMSD among the average structures of these families (Table 3). However, the penalty ratio in the run R3 is approximately twice as large as that of R2, whereas that of R4 was lower (0.24). By considering the penalty and RMSD, the δ used in R3 (0.5 Å) appears to generate too narrowly defined restraints, giving substantially increasing penalty without improving the structural precision. From the results of the best converging runs (R2 and R4), the optimal δ values are in the 1.0 to 1.5 Å range.

Testing the location of the helical center of rotation

Three of the five degrees of freedom imposed on the Cartesian transformation of the individual helices involve axial

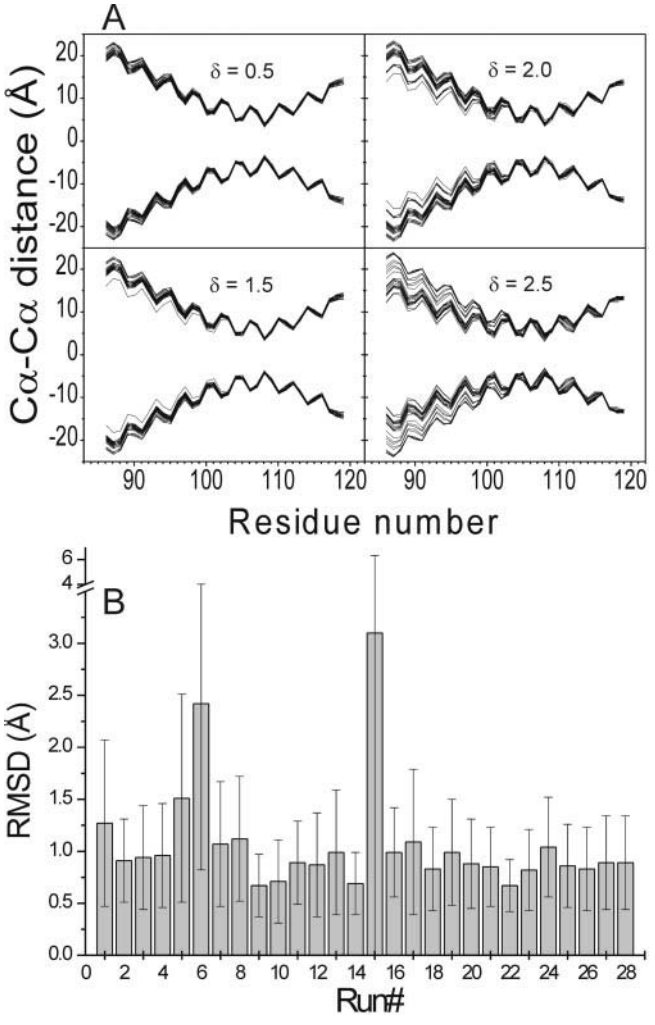

FIGURE 5 (*A*) The projected distance of the α-carbon diagonal-subunit of the 25 ReDCaT conformers obtained from the run R3 to R6. (*B*) Summary of the global RMSD for all runs (R1–R28) present in this report. The error bars correspond to standard deviation of RMSD values.

tilts. Because of this, we set out to test the influence of the location of center of rotation in each TM2 helix on the intra-ensemble deviations. In the R1 to R6 runs, the α-carbon of the residue 86 was defined as the center of rotation of each subunit. The following seven runs, R8 to R14, tested sequential locations for the rotating center according to the α-carbon of the following six residues: 90, 95, 100, 108, 113, 119, and an additional one at the center of mass of the TM2 segment. Again, these runs were carried out using the same dataset and search conditions as those used in R2. Remarkably, results of R8 to R14 (Table 4) suggest that the helical center of rotation has a negligible influence in the ensemble deviations, as the structures of all compared ensembles are practicably indistinguishable from each other. The pairwise RMSD values among the average structures of R2 and R8 to R14 extended from 0.09 to 0.67 Å, suggesting the same transmembrane helix packing. The results indicate that the efficiency of the ReDCaT sampling configurations is not influenced by the defined center of the TM rotations. Any rotating centers can be chosen.

TABLE 3 Pairwise RMSD values (Å) between the average structures of R1 to R6

	⟨R1⟩	⟨R2⟩	⟨R3⟩	⟨R4⟩	⟨R5⟩	⟨R6⟩
⟨R1⟩		0.83	0.79	0.66	0.47	0.98
⟨R2⟩			0.12	0.22	0.47	1.67
⟨R3⟩				0.27	0.46	1.63
⟨R4⟩					0.27	1.49
⟨R5⟩						1.22
⟨R6⟩						

Comparison with crystal structure

As a way to directly compare the ensemble deviations of ReDCaT-generated structures with *KcsA* crystal structure, we require an equivalent TM2 bundle structure in the closed state. This can be obtained by performing a backward run, in which the starting reference structure was in the open state and the ReDCaT protocol was applied reversing the sign and the distance range of the restrains. The backward run, R7, was carried out using the same search procedure as in R2. This is illustrated in Fig. 6, in which the original closed TM2 bundle (derived from the crystal structure) is shown in red, the open ReDCaT structure in blue, and the closed ReDCaT structure in green, overlapped to the x-ray structure. The intra-family RMSD of 25 conformers in the closed state was 1.02 $\pm$ 0.3 Å, and showed an average backbone deviation of 0.65 Å with respect to the x-ray structure. These results illustrate that the back-calculated ReDCaT conformers are remarkably close to the x-ray structure and that the structure from the open conformation can be brought back to the closed conformation using the inversed restraints.

Sensitivity of the restraints

How does each restraint affect the calculation of the open model? To further understand the sensitivity of the SDSL-EPR restraints, 10 ReDCaT runs, R15 to R24, were performed eliminating one distance constraint each time. From this test, the observed RMSDs within the ensembles R16 to R24 were between 0.67 and 1.04, indicating the convergence of the selected conformers (Tables 5). However, the pairwise RMSD (Table 6) showed that some of these runs failed to provide an accurate model. Particularly, the precision and accuracy of R15 and R16 appear compromised. The pairwise RMSD of $\langle R15\rangle_{100}$ and $\langle R16\rangle_{103}$ with respect to the target increased to 8.25 and 9.08 Å, respectively. Consequently, distance restraints from residues 100 and 103 appear to be the critical to obtain accurate models.

In the case of R18, R19, and R22, RMSD comparison revealed that excluding the restraint from residues 108, 109,

TABLE 4 Pairwise RMSD values (Å) of the average structure of R2, R8 to R14

	$\langle R2\rangle^*_{c86}$	$\langle R8\rangle_{c90}$	$\langle R9\rangle_{c95}$	$\langle R10\rangle_{c100}$	$\langle R11\rangle_{c108}$	$\langle R12\rangle_{c113}$	$\langle R13\rangle_{c119}$	$\langle R14\rangle_{cms}$
$\langle R2\rangle_{c86}$		0.09	0.45	0.2	0.23	0.31	0.3	0.17
$\langle R8\rangle_{c90}$			0.49	0.28	0.3	0.37	0.35	0.24
$\langle R9\rangle_{c95}$				0.35	0.28	0.18	0.67	0.37
$\langle R10\rangle_{c100}$					0.09	0.18	0.32	0.12
$\langle R11\rangle_{c108}$						0.12	0.39	0.14
$\langle R12\rangle_{c113}$							0.5	0.23
$\langle R13\rangle_{c119}$								0.33
$\langle R14\rangle_{cms}$								

*The residue number denoted by the subscript indicates the selected α-carbon as a center of rotations. The cms refers to the center of mass of TM2 segment was used instead.

and 116 generated significant differences in TM packing compared with the target structure with pairwise RMSD of $\langle R18\rangle_{108}$, $\langle R19\rangle_{109}$, and $\langle R22\rangle_{116}$ being 1.38, 2.99, and 2.30 Å, respectively. For the R17, R20, R21, R23, and R24 runs, the ensembles were identical to that of R2, implying that these particular positions exert little influence on the overall quality of the structures and suggests that given the right choice of distances, equivalent structures can be obtained with fewer constraints. From this test, we conclude that the quality of the model depends not only on the number of restraints but also the choice of restraints.

Influence of the number of restraints

From the previous section it is clear that using fewer than the 10 available constraints still produced reliable bundle structures using ReDCaT. To specifically test the minimal number of constraints still tolerated by the method, a series of runs were generated in which restraints were taken out in pairs, threes, and up to five (R25–R28). The ensembles of these runs show the pairwise RMSDs in the range of 0.26 to 1.42 Å, suggesting that these individual runs converged fairly well, provided that the critical distance restraints (100 and 103) were included in the calculation (Table 7). Obviously, the intra-family deviations of these ensembles increase as the number of the restraints used in the calculation decrease. However, the effects of the sequential restrain deletion were not linearly additive, particularly in the runs with deletions of four and five restraints.

Calculated structures

From the tests described above, runs R2 and R4 appear to generate the best set of structures. Fifty structures obtained from these two ensembles were subjected to the refinement, and the results are summarizes in Table 8. Refinement resulted in a substantial improvement of the van der Waals and electrostatic energies (data not shown). In the refined models, ~91% of nonglycine and nonproline residues fall in the most favored regions of the Ramachandran diagram and no residue drops in the disallowed regions. The backbone RMSD of the final refined structure, $\langle refReDCaT\rangle_{min}$, compared with the ReDCaT structures, {ReDCaT}, indicates no significant change after the refinement (~1.3 Å). The tendency of diagonal distance changes for the refined structure is consistent to that of ⟨ReDCaT⟩ (Fig. 7).

Fig. 7 shows the magnitude and the direction of Cα diagonal distances of the calculated structures with respect to the x-ray structure and compared with the pH-dependent distance change (from pH 7 to pH 4) observed from the experimental EPR. Most of the distance change data from

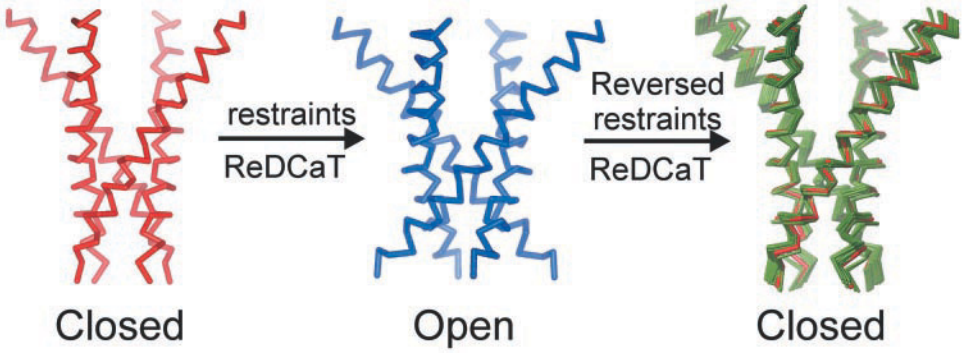

FIGURE 6 Backward calculation procedure: the x-ray crystal structure (*red*), the average open state (*blue*), and the back-calculated 25 ReDCaT conformers (*green*) superimposed with the x-ray structure.

TABLE 5 Global RMSD values (Å) within the ensemble of R15 to R24

R15	R16	R17	R18	R19	R20	R21	R22	R23	R24
3.10 ± 3.2	0.99 ± 0.4	1.09 ± 0.7	0.83 ± 0.4	0.99 ± 0.5	0.88 ± 0.4	0.85 ± 0.4	0.67 ± 0.3	0.82 ± 0.4	1.04 ± 0.5

the EPR experiments are in agreement with the direction of the mainchain movement of the calculated TM2 bundle. In this study, 7 of the 10 Cα-Cα distances were shifted with the same trend as the change of the interspin distances (residues 103, 109, 112, 115, 116, 117, and 119). The direction of interspin distance changes for residues 100, 107, and 108 is in apparent discrepancy with the results calculated from the ReDCaT, but the violations of the distance change in these restraints do not exceed 2 Å, considerably about the intrinsic resolution of the EPR-based distance determinations. With the exception of the magnitude in distance change for residue 109, the general tendency of the helical conformational change suggests a much larger separation at the C-terminal end of the helix. It is possible that in this particular position additional nitroxide side-chain rearrangements might be contributing to the observed inter-subunit distance change.

Conformational changes and structural features of the open channel model

Comparison of the helical rearrangements of TM2 between the *KcsA* crystal structure and the ReDCaT models are summarized in Table 8 and Figs. 8 and 9 . The backbone RMSD between the x-ray crystal structure and the average refined ReDCaT conformations was 3.4 Å. The position and orientation of the four segments in the open state derived from SDSL-EPR restraints reflect an approximate change in tilting and twisting of the inner transmembrane segments in the x-ray crystal structure (Fig. 8).

To provide a systematic structure analysis of conformational changes, we first introduced three fundamental components, $\Delta\theta_z$, $\Delta\theta_{xy}$, and $\Delta\theta_{hx}$ as a measurement of the helical reorientations in the two states. The sign of these components is regarded as directions of the TM2 movement with respect to the x-ray structure. From an extracellular point of view, a counterclockwise rotation about the axis of symmetry of the channel molecule corresponds to a negative $\Delta\theta_z$. On the other hand, the sign of $\Delta\theta_{xy}$ is defined by watching the domain movement from the lateral view. A positive $\Delta\theta_{xy}$ implies movement of TM2 toward the equatorial plane of bilayer (the *x-y* plane), whereas a negative sign suggests tilts toward the core axis. $\Delta\theta_{hx}$ measures the rotation of the helix itself and the definition for the sign of $\Delta\theta_{hx}$ is the same as that applied to $\Delta\theta_z$.

Upon pH-dependent activation, TM2 moves according to the following transformations: $\Delta\theta_z$ of $-8 \pm 3°$, $\Delta\theta_{xy}$ of $+8 \pm 3°$, and $\Delta\theta_{hx}$ of $-32 \pm 3°$. Therefore, the corresponding mechanical process of the inner helices in channel gating involves: 1) counterclockwise rotations around the virtual four-fold axis of symmetry (Fig. 8 *A*); 2) tilts of TM2 toward the *x-y* plane (Fig. 8 *B*); and 3) a counterclockwise helical rotation along the helical axis (Fig. 8). These results are in direct agreement with the types of molecular rearrangements proposed previously based on more qualitative data (Perozo et al., 1999).

An increasing of the helix-crossing angle (the angle between two diagonal TM2 bundles) ~16° suggests that a scissor-like motion is associated with channel gating. From the RMSD calculation between closed (crystal structure) and open ($\langle$refReDCaT$\rangle_{min}$) conformations (Fig. 9), the largest deviation occurs around the residues located near the cytoplasmic entrance. This includes residue V115-Q119. This clearly suggests that *KcsA* gating must be associated with a significant change in the diameter of the intercellular vestibule of the channel. By using a full-atom representation of the open TM2 bundle, the relative proximity changes between inter-subunit residues 116 to 119 further support this idea (Fig. 8 *C*). In the open state, the inter-subunit residues located around the upper portion (residues 101–105) pack relatively tighter than those in the closed state, whereas those near the intracellular side (residues 116–119) move apart from each other (Fig. 8 *C*). This generates a wide cytoplasmic cavity able to accept multiple water molecules and is likely to interact with larger channel blockers. The diameter at the narrowest point of the permeating pathway (residues 106–110) slightly increases (~1.0 Å), which likely favors the ion translocation process.

Testing alternative models

Because the open models before and after the structure refinement are only slightly different, we have further built additional models using ReDCaT to examine whether or not the magnitude and the direction obtained from our model represent the best solution to the open

TABLE 6* Pairwise RMSD values (Å) of the average structure of R15 to R24 with respect to the $\langle$R2$\rangle$

	$\langle R15\rangle_{100}$	$\langle R16\rangle_{103}$	$\langle R17\rangle_{107}$	$\langle R18\rangle_{108}$	$\langle R19\rangle_{109}$	$\langle R20\rangle_{112}$	$\langle R21\rangle_{115}$	$\langle R22\rangle_{116}$	$\langle R23\rangle_{117}$	$\langle R24\rangle_{119}$
$\langle$R2$\rangle$	8.25	9.08	0.63	1.38	2.99	0.03	0.56	2.30	0.12	0.40

*The subscript indicates the residue number from which the restraint was taken out.

TABLE 7 Pairwise RMSD values (Å) of the average structures of R25 to R28 with respect to ⟨R2⟩

	⟨R2⟩	Residue number*
⟨R25⟩	0.26	107, 119
⟨R26⟩	1.27	107, 115, 119
⟨R27⟩	1.42	107, 112, 115, 119
⟨R28⟩	1.42	107, 112, 115, 117, 119

*The residue number corresponds to restraints that were taken out from the calculations.

TM2 bundle structure. In this test, we used the restrained dataset with $\delta = 1.5$ Å and the values of the rotational parameters (θ_1–θ_4) were sequentially varied following a combinatorial approach, in such a way that new configurations were generated with the same magnitude of the mean values of $\Delta\theta_z$, $\Delta\theta_{xy}$, and $\Delta\theta_{hx}$ in Table 8. Here, only the translational parameter σ was varied to generate structures in each examined direction, and a total of five structures with the lowest penalty value was collected for each ensemble. A total of 12 ensembles including eight different directions (I–VIII) from the combination of the parameters plus additional four directions (IX–XII) were shown in Table 9. Fig. 10 shows the 12 ensembles of which the generated models (from light blue to blue) were superimposed with the x-ray structure (red).

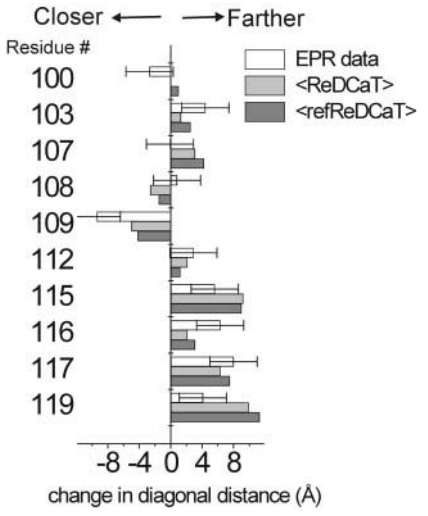

FIGURE 7 Diagonal distance changes from the closed to the open state for selected residues. Comparison between the changes in experimental interspin distances (EPR) and the mean Cα-Cα distances of {ReDCaT} and {refReDCaT}. Error bar represents the range of distance restraints.

With the exception of ensemble XI, the relative penalty of the ensemble I, the structures most similar to the final refined model, confirms that the structural rearrangements

TABLE 8 Structural statistics

	{ReDCaT}	{refReDCaT}	⟨refReDCaT⟩$_{min}$
Structural properties*			
Violation			
Average (Å)	0.7	1.0	0.8
Maximum (Å)	4.5	5.6	4.2
Number of violation >2.0 Å	1	1	1
Amber Total energies (kcal mol^{-1})	$10^8 - 10^{19}$	-3.3×10^3–-3.0×10^3	-3.1×10^3
Global RMSD (Å)			
Backbone	0.92 ± 0.50	1.13 ± 0.48	n/a
Heavy	1.07 ± 0.53	1.32 ± 0.52	
RMSD versus ⟨refReDCaT⟩$_{min}$ (Å)			
Backbone	1.30 ± 0.27	0.97 ± 0.32	n/a
Heavy	1.65 ± 0.25	1.24 ± 0.34	
Ramachandran plot statistics (%)			
Most favored regions	88.5	91.4	91.1
Additional allowed regions	11.5	8.6	8.9
Generously allowed regions	0	0	0
Disallowed regions	0	0	0
Structure comparison to the x-ray crystal structure			
RMSD (Å)			
Backbone	3.57 ± 033 (3.07 − 4.40)	3.46 ± 033 (2.82 − 4.16)	3.37
Heavy	4.21 ± 031 (3.62 − 4.83)	4.14 ± 032 (3.50 − 4.60)	4.02
Helix tilting angle†			
$\Delta\theta_{xy}$	+8 ± 3°	+9 ± 3°	+8°
$\Delta\theta_z$	−8 ± 3°	−8 ± 3°	−8°
Helix twisting angle† ($\Delta\theta_{hx}$)	−33 ± 3°	−32 ± 3°	−32°

*{ReDCaT} and {refReDCaT} are the ensemble of 50 structures before and after energy minimization, respectively. ⟨refReDCaT⟩$_{min}$ is the energy minimized structure averaged from {refReDCaT}.
†The + sign represents the clockwise rotation (see text for details).

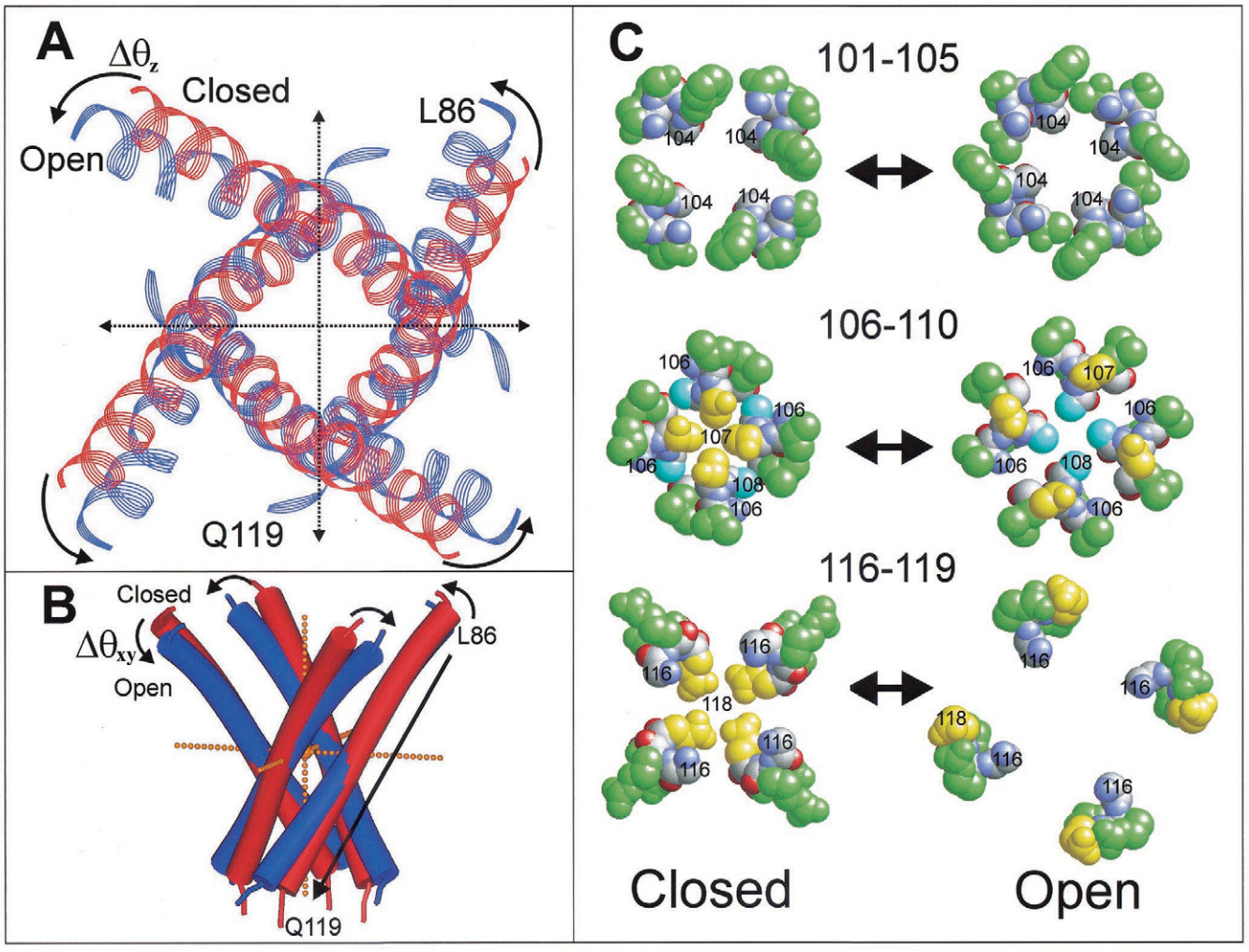

FIGURE 8 Proposed model for the structural rearrangements of the four inner helices upon activation gating. *A* and *B* illustrate the rotation of TM2 segments from the closed (*red*) to the open (*blue*) states. $\Delta\theta_z$ and $\Delta\theta_{xy}$ are described in the text. (*C*) Spacefill representation showing an orientation of residue in three different regions, 101–105, 106–110, and 116–119. For clarification, the sidechain atoms are colored in green and yellow.

are most consistent to the SDSL-EPR restraints. As illustrated by ensemble II (only $\Delta\theta_{hx}$ has an opposite sign with respect to the ensemble I), a clockwise rotation about the segment itself produces a dramatic increase in restrain vio-

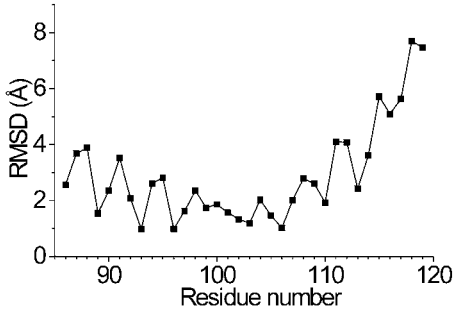

FIGURE 9 Backbone RMSD per residues between the closed (x-ray) and the open $\langle \text{refReDCaT} \rangle_{min}$ conformations.

TABLE 9* Relative penalty of the 12 ensembles

Ensemble	$\Delta\theta_z$	$\Delta\theta_{xy}$	$\Delta\theta_{hx}$	Relative penalty†
I	−	+	−	1.0
II	−	+	+	6.5
III	−	−	−	7.1
IV	−	−	+	8.5
V	+	+	−	1.4
VI	+	+	+	5.5
VII	+	−	−	17.3
VIII	+	−	+	11.0
IX	−	0°	−	2.5
X	+	0°	−	7.4
XI	0°	+	−	0.9
XII	0°	−	−	11.3

*The sign indicates a direction of rotation as defined in text and Table 8. 0° means no rotation.

†Relative penalty is the absolute penalty divided by the absolute penalty of the ensemble I. The absolute penalty is an average penalty calculated from five selected ReDCaT models.

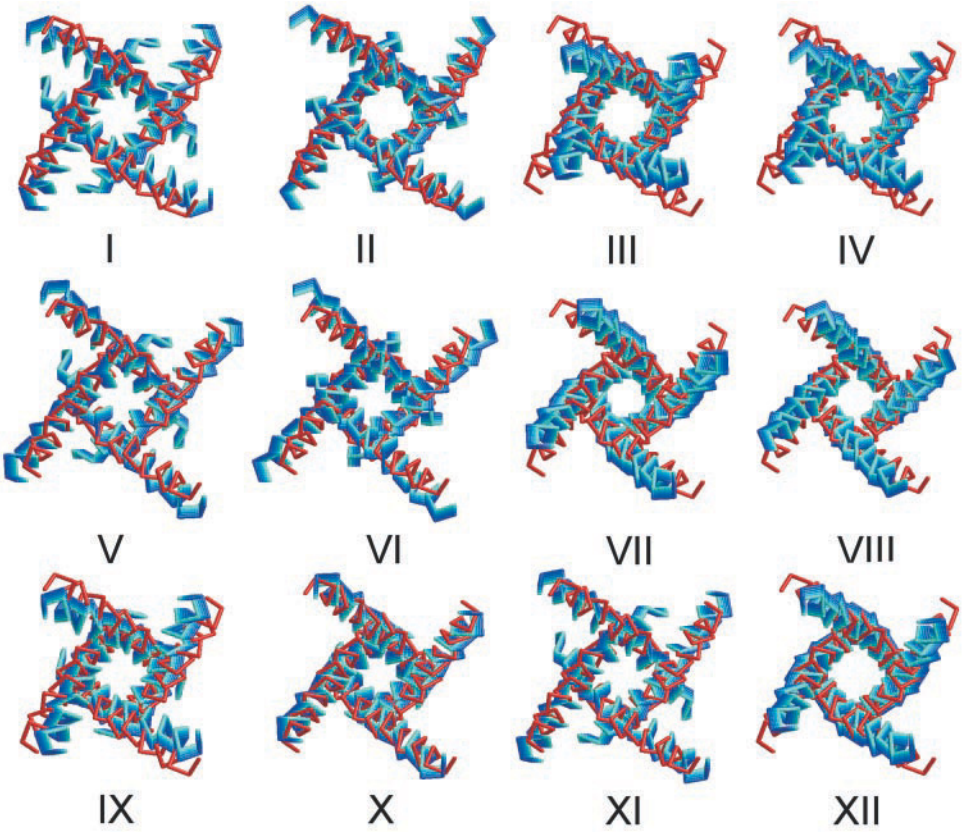

FIGURE 10 Cα traces of the tested models (shading from *light blue* to *blue*) for 12 different ensembles. Each ensemble was superimposed onto the x-ray crystal structure (*red*).

lation, again suggesting that counterclockwise rotation of the helix itself is best supported by the data. Similarly, ensemble III demonstrates that a helical tilt toward the axis of symmetry is very unfavorable (also seen in ensemble IV). The models from a clockwise rotation in ensemble V are of interest because of an increase of ~40% of the relative penalty. However, it became even worse when the magnitude of clockwise rotation increased (data not shown). The other three ensembles VI to VIII strongly disagree to SDSL-EPR restraints. Again, the two most inconsistent models compose of the positive $\Delta\theta_z$ (clockwise rotation) and the negative $\Delta\theta_{xy}$ (move toward the axis) as shown the ensemble VII and VIII. In addition, four additional ensembles IX to XII were generated for the same purpose. The failure of the ensembles IX, X, and XII was due to the higher relative penalties with respect to that of the ensemble I.

From the model test, the relative penalty of ensemble XI is slightly lower than that of the ensemble I. Both two ensembles are similar except for no tilting along the *z* axis. It is difficult to analyze these differences quantitatively because they are very small. A fine search for $\Delta\theta_z$ in the range of $+8°$ to $-8°$ suggested that the minimum of the penalty was obtained between $-4°$ and $-6°$, implying that more favorable models include the counterclockwise rotation about the axis. From this test, the direction and magnitude of the tilt and the twist confirm the results in Table 8 and are taken as the best answers for the conformational changes based on the SDSL-EPR data.

DISCUSSION

Despite recent spectacular successes, high-resolution structural determinations of membrane proteins by means of traditional structural methods (x-ray crystallography, multidimensional NMR) remains a challenging problem. A number of alternative, lower resolution approaches have shown great promise in elucidating the overall structural properties of these complex systems, particularly in relation to functionally relevant conformational changes. Reporter group techniques represent a very attractive approach to provide structural information in membrane protein systems because the data are generally obtained at room temperature, in membrane-embedded conditions, and in physiological solutions. A number of examples document the application of site-directed spin labeling (SDSL-EPR) and the use of fluorescent probes to attack structural problems in membrane proteins (Hubbell et al., 2000; Selvin, 2000;

Weiss, 2000). One key disadvantage, however, is that the number of SDSL-EPR restraints (and other reporter-group techniques) in a given system is limited by the efficiency of the protein expression, labeling, and purification steps. Thus, each SDSL-EPR sample produces only one distance information, and this information in limited to the level of the backbone fold.

A number of efforts for calculating the global fold of protein structures using a small number of restraints have been reported (Smith-Brown et al., 1993; Aszodi et al., 1995; Skolnick et al., 1997). These methods can produce adequate tertiary folds of monomeric proteins from an extended protein chain. However, the atomic resolution of models generated by the methods is typically low to moderate with RMSD > 4.0 Å. Conformational rearrangements at this resolution may be hard to detect using these methods. Additionally, it will be difficult to assess the model quality required for analysis of the structure-function relationship that is important step toward the elucidation of function.

In this study we have introduced ReDCaT, an approach for calculating structural rearrangements in membrane proteins using few numbers of distance data. The framework of our method was adapted based on the limited availability of experimental information. Parameterizations were performed to find out appropriate computational strategies compromising between the level of the experimental quality, the structural features of the system studied, and the assumptions used in the approach. ReDCaT has several advantages when compared with other computational methods using distance constraints. The use of Cα (or Cβ) distance changes instead of absolute interspin distances by giving a 6 Å ($\delta = 1.5$ Å) distance deviation results in a much-simplified approach without the complicated treatment for the spin label sidechain. Additionally, distance data from different mutants can be used as part of the same SDSL-EPR restraint dataset because the restraints are, in many cases, independent of the spin probe conformation. Thus, only a single model representing the backbone polypeptide is needed by assuming little or no mainchain perturbations due to the mutagenesis and spin labeling.

In determining a given conformational change, knowledge of a reference structure is critical because the initial coordinates are used twofold: 1) as a structural transmembrane template and 2) as a source for penalty calculations. Another useful feature of the approach is that the use of the rigid body transformation and the symmetric relationship reduces substantially the searchable space, resulting in a simple and rapid sampling method.

The approach presented here is generally applicable in the analysis of conformational changes of membrane protein systems. At present, the computational procedure is well adapted to members of the voltage-dependent channel superfamily because of their similarity of the structural features: the four-fold symmetry relationship, the homologous repeating subunits, and the rigid body movement. We expect that this approach can also be applied to other nonsymmetric membrane proteins such as bacteriorhodopsin and members of the G-protein-coupled receptor superfamily, because there is clear evidence pointing to helical rigid-body movements upon ligand activation (Farrens et al., 1996; Subramaniam and Henderson, 2000).

It should be noted that analysis of probe dynamics and the use of accessibility parameters from the power saturation EPR spectra have great potential to be used as additional structural restraints. It has been shown that these parameters are proportional to the solvent exposed surface area of proteins (Mchaourab et al., 1996; Mchaourab and Perozo, 2000; Columbus et al., 2001). Although implementing this approach would require a large number of cysteine-mutants, the relationship between geometric methods and additional solvent accessibility constraints is worth exploring in the near future. In this case, the initial reference structure may no longer be needed to calculate secondary structures and tertiary folds. Furthermore, these restraints would be also applicable to soluble proteins. Incorporating these types of restraints would fulfill some deficiencies of our approach, enabling to calculate more accurate models.

Limitations and caveats of the method

Although it is clear that the ReDCaT approach is able to generate reliable information regarding the structural basis of conformational changes in membrane proteins, the method has intrinsic limitations that must be taken into account when applied to different systems. One important caveat is the requirement for an initial reference structure. This will certainly limit the generality of the approach, because obtaining medium-to-high resolution structures of membrane proteins is still a challenging problem.

A key consideration in the generalized use of reporter group techniques as a source of structural constraints is not only the possible perturbations that the probe might generate, but also the intrinsic difficulty in correlating changes in inter-probe distances with actual changes in inter-residue distances. One should keep in mind that a measurable change in interspin distance involves three possible processes: motion of the backbone, motion of the sidechain, or both. This remains an unresolved problem in the use of spin labels or fluorescent probes. However, recent analysis of spin label conformations by x-ray crystallography strongly suggest that for the standard methanethiosulfonate spin label (that used in generated the present data set), the nitroxide side chain adopts a fairly compact structure and never populate a large range of its conformational space (Langen et al., 2000). In fact, these results tend to confirm the empirically determined value of δ in the 1.0 to 1.5 Å range and suggest that the spin dipole in the nitroxide sidechain located within 5 Å of the Cα.

The rigid body approach appears to be appropriate, particularly in membrane protein systems because transmem-

brane segments are unlikely to undergo major changes in secondary structure during conformational changes. By taking advantage of the predicted four-fold symmetry of ion channels, it is reasonable to assume that restraints based on multiple distance changes along a rigid body segment would be able to overcome the limited accuracy of individual distance data during structure calculations. As shown in this report, these assumptions, combined with proper ranges for the distance boundaries, appear to produce consistent results.

An additional factor to consider is the need to further refine the resulting structures from ReDCaT by evaluating potential energy functions of the ensemble average, because the method is purely geometric (Sansom and Kerr, 1993; Sansom et al., 1997). We found that the steric conflicts between clashing residues of neighboring helices were eliminated with a simple refinement step. Although the refined structure still agrees with the experimental restraints, gaining of nonbonding energy was achieved at the expense of slight increases in the value of the penalty function (Table 8). A reverse ReDCaT run using the sterically refined open gate model revealed that the RMSD between the x-ray crystal structure and the new closed average model increased slightly to ~0.7 Å. Thus, ReDCaT is robust, and the refinement does not generate substantial alteration of the structure.

CONCLUSION

A novel approach to determine the conformational rearrangement of the membrane proteins using a small number of SDSL-EPR restraints was proposed. The method is simple, rapid, and needs only the limited information from this reporter group techniques to derive reliable conformational changes of the proteins. Two important aspects are highlighted. On one hand, the development of a strategy is to use experimental information from SDSL-EPR experiments to calculate rigid-body movements of membrane proteins in three dimensions. Second, use of this approach allowed us to propose a molecular description of the structural rearrangement of the potassium *KcsA* channel upon activation gating. The present study demonstrates that ReDCaT can be very useful in the analysis of conformational rearrangement of membrane proteins.

APPENDIX

Alternative distance evaluation in ReDCaT

In developing ReDCaT, we considered using the distance ratio instead of the distance difference in evaluating the use of experimental distances. The approach is described as follows.

For any two interacting spins, the intensity of the electron-electron dipolar coupling is related to interspin separation as

$$I_c = C/r_c^3 \tag{A1}$$

in which C is a constant, and r_c is the distance between the two spin labels in the closed state. Using the analogous consideration for the open state, the ratio (τ) of the EPR signal from the same spin-spin interactions in the open and the closed states is estimated as

$$\tau = I_o/I_c = (r_c/r_o)^3 \tag{A2}$$

Applying Eq. A2 to the experimental EPR distance dataset, we can set up a new set of restraints for the distance ratio as:

$$\tau_{epr} = (r_{pH7}/r_{pH4})^3 \tag{A3}$$

$$\tau_{upl} \text{ and } \tau_{lol} = \tau_{epr} \pm \delta \tag{A4}$$

Similarly to the distance difference approach, δ is used to generate the range between the upper and the lower distance bounds. The only difference is that here, δ represents the percentage of the τ_{epr} deviation. The violation function for the ratio restraint was similar to that defined for the distance difference restraint as:

$$viol = \begin{cases} \tau_{calc} - \tau_{upl}; & \tau_{calc} > \tau_{upl} \\ \tau_{lol} - \tau_{calc}; & \tau_{calc} < \tau_{lol} \\ 0; & \tau_{lol} \le \tau_{calc} \le \tau_{upl} \end{cases} \tag{A5}$$

$$\tau_{calc} = (r_{x\text{-}ray}/r_{ReDCaT})^3 \tag{A6}$$

Thus, we ran ReDCaT with δ varying 10, 20, 30, and 40% of τ_{epr}. An evaluation of intra-family RMSD and the penalty indicates that the optimal value of δ falls between 20 to 30%. As expected, the most divergent part is the extracellular region owing to the lack of experimental restraints. Nevertheless, the models generated from the distance ratio and the distance difference approaches produce similar TM rearrangements that include helical tilting, the counterclockwise rotation, and an increase in the diameter around the cytoplasmic entrance.

We thank Dr. Benoit Roux for many insightful comments and for the suggestion to use distance ratios for penalty evaluation. We thank L. Cuello, D. Cortes, C. Ptak, Y. Shen, and A. Sompornpisut for their useful comments. P.S. would like to express an appreciation to Chulalongkorn University and Office of the Civil Service Commission, Thailand for supporting research training abroad.

This work was supported by National Institutes of Health and the McKnight Endowment Fund.

REFERENCES

Allen, T. W., A. Bliznyuk, A. P. Rendell, S. Kuyucak, and S.-H. Chung. 2000. The potassium channel: structure, selectivity and diffusion. *J. Chem. Phys.* 112:8205–8206.

Aqvist, J., and V. Luzhkov. 2000. Ion permeation mechanism of the potassium channel. *Nature.* 404:881–884.

Aszodi, A., M. J. Gradwell, and W. R. Taylor. 1995. Global fold determination from a small number of distance restraints. *J. Mol. Biol.* 251: 308–326.

Berneche, S., and B. Roux. 2000. Molecular dynamics of the KcsA K(+) channel in a bilayer membrane. *Biophys. J.* 78:2900–2917.

Booth, P. J., and A. R. Curran. 1999. Membrane protein folding. *Curr. Opin. Struct. Biol.* 9:115–121.

Bowie, J. U. 1997a. Helix packing angle preferences. *Nat. Struct. Biol.* 4:915–917.

Bowie, J. U. 1997b. Helix packing in membrane proteins. *J. Mol. Biol.* 272:780–789.

Capener, C. E., I. H. Shrivastava, K. M. Ranatunga, L. R. Forrest, G. R. Smith, and M. S. Sansom. 2000. Homology modeling and molecular dynamics simulation studies of an inward rectifier potassium channel. *Biophys. J.* 78:2929–2942.

Case, D., D. Pearlman, J. Caldwell, T. Cheatham, III, W. Ross, C. Simmerling, T. Darden, K. Merz, R. Stanton, A. Cheng, J. Vincent, M. Crowley, V. Tsui, R. Radmer, Y. Duan, J. Pitera, I. Massova, G. Seibel, U. Singh, W. P., and P. Kollman. 1999. AMBER 6, University of California, San Francisco.

Columbus, L., T. Kalai, J. Jeko, K. Hideg, and W. L. Hubbell. 2001. Molecular motion of spin labeled side chains in alpha-helices: analysis by variation of side chain structure. *Biochemistry.* 40:3828–3846.

Cornell, W. D., P. Cieplak, C. J. Bayly, I. R. Gould, K. M. Merz, Jr., D. M. Ferguson, D. C. Spellmeyer, T. Fox, J. W. Caldwell, and P. A. Kollman. 1995. A second generation force field for the simulation of proteins, nucleic acid, and organic molecules. *J. Am. Chem. Soc.* 117:5179–5197.

Cortes, D. M., L. G. Cuello, and E. Perozo. 2001. Molecular architecture of full-length *KcsA*: role of cytoplasmic domains in ion permeation and activation gating. *J. Gen. Physiol.* 117:165–180.

Cortes, D. M., and E. Perozo. 1997. Structural dynamics of the *Streptomyces lividans* K+ channel (Skc1): oligomeric stoichiometry and stability. *Biochemistry.* 36:10343–10352.

Cuello, L. G., J. G. Romero, D. M. Cortes, and E. Perozo. 1998. pH-dependent gating in the *Streptomyces lividans* K+ channel. *Biochemistry.* 37:3229–3236.

Donnelly, D., J. P. Overington, S. V. Ruffle, J. H. Nugent, and T. L. Blundell. 1993. Modeling alpha-helical transmembrane domains: the calculation and use of substitution tables for lipid-facing residues. *Protein Sci.* 2:55–70.

Doyle, D. A., J. M. Cabral, R. A. Pfuetzner, A. Kuo, J. M. Gulbis, S. L. Cohen, B. T. Chait, and R. MacKinnon. 1998. The structure of the potassium channel: molecular basis of K+ conduction and selectivity. *Science.* 280:69–77.

Eaton, G. R., and S. S. Eaton. 1989. Resolved electron-electron spin-spin splittings in EPR spectra. *In* Biological Magnetic Resonance. L. J. A. R. Berliner, editor. Plenum Publishing Corp., New York. 340–397.

Farrens, D. L., C. Altenbach, K. Yang, W. L. Hubbell, and H. G. Khorana. 1996. Requirement of rigid-body motion of transmembrane helices for light activation of rhodopsin. *Science.* 274:768–770.

Guidoni, L., V. Torre, and P. Carloni. 2000. Water and potassium dynamics inside the KcsA K(+) channel. *FEBS Lett.* 477:37–42.

Herzyk, P., and R. E. Hubbard. 1995. Automated method for modeling seven-helix transmembrane receptors from experimental data. *Biophys. J.* 69:2419–2442.

Herzyk, P., and R. E. Hubbard. 1998. Using experimental information to produce a model of the transmembrane domain of the ion channel phospholamban. *Biophys. J.* 74:1203–1214.

Hubbell, W. L., and C. Altenbach. 1994. Site-directed spin labeling of membrane proteins. Oxford University Press, New York.

Hubbell, W. L., D. S. Cafiso, and C. Altenbach. 2000. Identifying conformational changes with site-directed spin labeling. *Nat. Struct. Biol.* 7:735–739.

Hubbell, W. L., A. Gross, R. Langen, and M. A. Lietzow. 1998. Recent advances in site-directed spin labeling of proteins. *Curr. Opin. Struct. Biol.* 8:649–656.

Hustedt, E. J., A. I. Smirnov, C. F. Laub, C. E. Cobb, and A. H. Beth. 1997. Molecular distances from dipolar coupled spin-labels: the global analysis of multifrequency continuous wave electron paramagnetic resonance data. *Biophys. J.* 72:1861–1877.

Koradi, R., M. Billeter, and K. Wuthrich. 1996. MOLMOL: a program for display and analysis of macromolecular structures. *J. Mol. Graph.* 14: 51–55.

Koteiche, H. A., and H. S. McHaourab. 1999. Folding pattern of the alpha-crystallin domain in alphaA-crystallin determined by site-directed spin labeling. *J. Mol. Biol.* 294:561–577.

Kraulis, P. J. 1991. MOLSCRIPT: a program to produce both detailed and schematic plots of protein structures. *J. Appl. Crystallogr.* 24:946–950.

Kukol, A., P. D. Adams, L. M. Rice, A. T. Brunger, and T. I. Arkin. 1999. Experimentally based orientational refinement of membrane protein models: a structure for the influenza A M2 H+ channel. *J. Mol. Biol.* 286:951–962.

Langen, R., K. J. Oh, D. Cascio, and W. L. Hubbell. 2000. Crystal structures of spin labeled T4 lysozyme mutants: implications for the interpretation of EPR spectra in terms of structure. *Biochemistry.* 39: 8396–8405.

Laskowski, R. A., J. A. Rullmannn, M. W. MacArthur, R. Kaptein, and J. M. Thornton. 1996. AQUA and PROCHECK-NMR: programs for checking the quality of protein structures solved by NMR. *J. Biomol. NMR.* 8:477–486.

Likhtenshtein, G. I. 1976. Spin Labeling Methods in Molecular Biology. John Wiley & Sons, New York.

Liu, Y-S., P. Sompornpisut, and E. Perozo. 2001. Structure of KcsA intracellular gate in the open state. *Nat. Struct. Biol.* 8:883–887.

Mchaourab, H., and E. Perozo. 2000. Determination of protein folds and conformational dynamics using spin-labeling EPR spectroscpy. *In* Distance Measurements in Biological EPR. G. Eaton, S. Eaton, and L. Berliner, editors. Kluwer Academic Publishers, New York.

Mchaourab, H. S., M. A. Lietzow, K. Hideg, and W. L. Hubbell. 1996. Motion of spin-labeled side chains in T4 lysozyme: correlation with protein structure and dynamics. *Biochemistry.* 35:7692–7704.

Pappu, R. V., G. R. Marshall, and J. W. Ponder. 1999. A potential smoothing algorithm accurately predicts transmembrane helix packing. *Nat. Struct. Biol.* 6:50–55.

Perozo, E., D. M. Cortes, and L. G. Cuello. 1998. Three-dimensional architecture and gating mechanism of a K+ channel studied by epr spectroscopy. *Nat. Struct. Biol.* 5:459–469.

Perozo, E., D. M. Cortes, and L. G. Cuello. 1999. Structural rearrangements underlying K+-channel activation gating. *Science.* 285:73–78.

Pogozheva, I. D., A. L. Lomize, and H. I. Mosberg. 1997. The transmembrane 7-alpha-bundle of rhodopsin: distance geometry calculations with hydrogen bonding constraints. *Biophys. J.* 72:1963–1985.

Poirier, M. A., W. Xiao, J. C. Macosko, C. Chan, Y. K. Shin, and M. K. Bennett. 1998. The synaptic SNARE complex is a parallel four-stranded helical bundle. *Nat. Struct. Biol.* 5:765–769.

Rabenstein, M. D., and Y. K. Shin. 1995. Determination of the distance between two spin labels attached to a macromolecule. *Proc. Natl. Acad. Sci. USA.* 92:8239–8243.

Roux, B., and R. MacKinnon. 1999. The cavity and pore helices in the KcsA K+ channel: electrostatic stabilization of monovalent cations. *Science.* 285:100–102.

Sansom, M. S. 1998. Models and simulations of ion channels and related membrane proteins. *Curr. Opin. Struct. Biol.* 8:237–244.

Sansom, M. S., and I. D. Kerr. 1993. Influenza virus M2 protein: a molecular modelling study of the ion channel. *Protein Eng.* 6:65–74.

Sansom, M. S., I. D. Kerr, G. R. Smith, and H. S. Son. 1997. The influenza A virus M2 channel: a molecular modeling and simulation study. *Virology.* 233:163–173.

Sansom, M. S., R. Sankararamakrishnan, and I. D. Kerr. 1995. Modelling membrane proteins using structural restraints. *Nat. Struct. Biol.* 2:624–631.

Sayle, R. 1994. Rasmol. Biomolecular Structure Department, Glaxo Research and Development, Greenford, Middlesex, UK.

Selvin, P. R. 2000. The renaissance of fluorescence resonance energy transfer. *Nat. Struct. Biol.* 7:730–734.

Shrivastava, I. H., and M. S. Sansom. 2000. Simulations of ion permeation through a potassium channel: molecular dynamics of KcsA in a phospholipid bilayer. *Biophys. J.* 78:557–570.

Skolnick, J., A. Kolinski, and A. R. Ortiz. 1997. MONSSTER: a method for folding globular proteins with a small number of distance restraints. *J. Mol. Biol.* 265:217–241.

Smith-Brown, M. J., D. Kominos, and R. M. Levy. 1993. Global folding of proteins using a limited number of distance constraints. *Protein Eng.* 6:605–614.

Son, H. S., and M. S. Sansom. 1999. Simulation of the packing of idealized transmembrane alpha-helix bundles. *Eur. Biophys. J.* 28:489–498.

Steinhoff, H. J., and W. L. Hubbell. 1996. Calculation of electron paramagnetic resonance spectra from Brownian dynamics trajectories: application to nitroxide side chains in proteins. *Biophys. J.* 71:2201–2212.

Steinhoff, H. J., N. Radzwill, W. Thevis, V. Lenz, D. Brandenburg, A. Antson, G. Dodson, and A. Wollmer. 1997. Determination of interspin distances between spin labels attached to insulin: comparison of electron paramagnetic resonance data with the x-ray structure. *Biophys. J.* 73: 3287–3298.

Subramaniam, S., and R. Henderson. 2000. Molecular mechanism of vectorial proton translocation by bacteriorhodopsin. *Nature* 406: 653–657.

Tatulian, S. A., D. M. Cortes, and E. Perozo. 1998. Structural dynamics of the *Streptomyces lividans* K+ channel (Skc1): secondary structure characterization from FTIR spectroscopy. *FEBS Lett.* 423:205–212.

Weiss, S. 2000. Measuring conformational dynamics of biomolecules by single molecule fluorescence spectroscopy. *Nat. Struct. Biol.* 7:724–729.

White, S. H., and W. C. Wimley. 1999. Membrane protein folding and stability: physical principles. *Annu. Rev. Biophys. Biomol. Struct.* 28: 319–365.